MULTI-CHANNEL CELL TO IRRADIATE THE MATERIAL SPECIMENS BY ELECTRONS IN THE INTERIOR OF THE SUPERCRITICAL WATER CONVECTION LOOP

A.S. Bakai, V.N. Boriskin, M.I. Bratchenko, Yu.V. Gorenko, A.N. Dovbnya, S.V. Dyuldya, G.G. Kovalev

National Science Center "Kharkov Institute of Physics and Technology", Kharkov, Ukraine
E-mail: gorenko@kipt.kharkov.ua

The 1.2×1.5 m sized Supercritical Water Convection Loop with four-channel irradiation cell was created in KIPT. The stainless steel made plant opens the possibility to carry out simulation corrosion tests of candidate structural materials for Generation IV Supercritical Water-Cooled Reactors (SCWR) under irradiation. Specimens in water flow at 350…400°C, 23…25 MPa are irradiated by 10 MeV/10 kW electron beam of LPE-10 linear accelerator. The results of the four-channel cell application for 500 hours long irradiation Zr and Inconel samples are presented.
PACS: 07.35.+k;29.20.Ej;28.52.Fa

INTRODUCTION

In 2010-2012, the convection loops were specially developed, in KIPT, for *in situ* investigations of combined influence of ionizing irradiation and heterophase fluctuations of the supercritical water (SCW) environment on corrosion, oxidation, and mechanical properties of metals and alloys. The irradiation cell (IC) equipped Supercritical Water Convection Loop (SCWCL) was coupled to the 10 MeV, 10 kW electron accelerator LPE-10 as a basis for the test bench of the Canada-Ukraine Electron Irradiation Test Facility (CU-EITF) for corrosion tests of structural materials of Generation IV Supercritical Water-Cooled Reactors (SCWR) [1, 2].

Three SCWCL models were developed and manufactured:

a) the SCWCL prototype without an irradiation cell,

b) all-welded SCWCL with four-channel IC, *and*

c) dismountable SCWCL with the circulation pump and the IC made from the titanium alloy VT22.

The pipes of all the devices (a–c) and the IC of the SCWCL model (b) were made from the 12X18H10T stainless steel. The internal volume of each loop was about 4 liters.

Dimensions of the loops (1.2×1.5 m, Fig. 1) and other component parts of SCWCLs were essentially determined by the size and arrangement of the KIPT sited bunker room (Fig. 2) which houses the electron accelerator LPE-10.
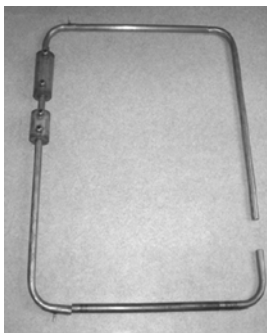

Fig. 1. The SCWCL prototype piping elements

Fig. 2. Placement of SCWCL in the bunker room of the LPE-10 electron linac

1. THE MULTI-CHANNEL IRRADIATION CELL DESIGN

In our case, the IC dimensions were identified reasoning from the parameters of the LPE-10 linac scanning electron beam, the dimensions of the SCWCL pipes, and the strength properties of the IC material.

To ensure the materials compatibility and the durability of welded joints of the all-welded SCWCL model (b), the same material, the stainless steel 12X18H10T, was chosen for both IC and SCWCL piping.

The LPE-10 scanning e^--beam area is about 210 mm high and about 45 mm wide. Respectively, the length of 4-channel IC of 300 mm was chosen taking into account some extra inventory (flanges, Fig. 3).

Starting from the evaluated range, in steel, of ~10 MeV primary e^--beam of the LPE-10 linac, it was identified that the IC channel wall thickness shall not exceed 2 mm to obtain significant irradiation effects [3] in the channel hosted samples under investigation.

Due to certain technological and economical limitations, the projected duration of the SCWCL relevant irradiations shall not exceed 1000 hours. Therefore, conservative evaluation of the IC durability under excessive internal pressure was undertaken for ~10^4 h long operation. Corrosion wear was also included according to the following formula [4]:

$$s = s_0 + C, \qquad (1)$$

where s_0 is the estimated thickness of a wall, mm, C is an increase to estimated thickness on corrosion, mm.

Fig. 3. Details of the 4-channel camera for SCWCL

For the collectors made of one or several seamless pipes, on the ends of the direct sections chiseled under

abutment welding thinning of a wall, the minimum allowed thickness of a wall of the direct pipe was calculated using the following formula [4]:

$$s_0 = \frac{pD}{2\varphi[\sigma_{allow}] + p}, \qquad (2)$$

where p is the internal pressure in the pipeline, MPa, D is the pipe outer diameter, mm, φ is the seam durability coefficient ($\varphi = 1$ for seamless pipes), σ_{allow} is the nominally allowable bursting stress, MPa, which is prescribed, by regulations [4], subject to the pipe steel grade and the temperature of a transported product.

For our case (steel 12X18H10T, operation resource 10^4 h at 500°C), the lookup value $\sigma_{allow} = 104$ MPa and the calculated $s(D)$ is shown in Fig. 4 for the utmost value of internal pressure $p = 30$ MPa. As a result, the 14 mm outer diameter of all IC channels was chosen at a thickness of walls of 2 mm.
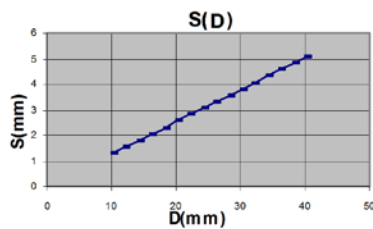

Fig. 4. The estimated allowed thickness s of a wall as a function of the outside diameter D of a steel pipe

The number of IC channels was fixed to 4 from the following reasons. First, such a layout allows to obtain a desirably non-uniform distribution of e^--beam fluence (e^-/cm^2) in different channels of the IC in course of a single irradiation. Next, the total internal cross-section of four-pipe IC is only about a half of that of the SCWCL pipe of internal diameter 32 mm. At a given mass-flow rate W of the SCWCL steady-state circulation of sub- or super-critical coolant, such a ratio results in an about twofold increase the linear velocity v of a water flow in each of IC channels hosting the tested samples. Generally, this enhances the corrosion kinetics of materials under investigation [5].

2. RESULTS OF IC SIMULATION

The reference energy spectrum of the LPE-10 scanning e^--beam typical for 10 MeV linac operation at 8…10 kW is shown in Fig. 5. Note the tail spreading to 12 MeV. It leads to the pronounced deviation of the target gamma fluence (and activation) from the predictions of δ-shaped model of electron energy distribution.
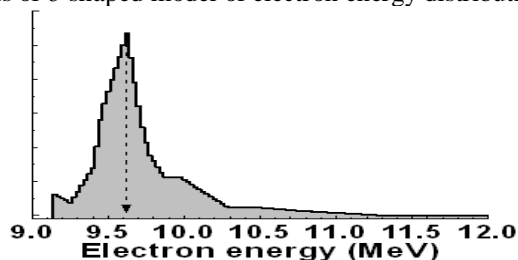

Fig. 5. Reference shape of the LPE-10 linac e-beam energy spectrum

The spatial distribution of the scanning beam has been parameterized basing on actual measurements which are periodically carried out by the LPE-10 linac crew. The short exposure of the glass plate located at a

well established position is routinely used to obtain the snapshot of the absorbed dose deposition. It is well scaled with the electron flux since the contribution of γ-quanta to the plate blackening (photographic density) is small in the geometry of the measurements.

The negative scans of exposed plates have been digitized to 16-bit levels of grey. The digital image processing technique has allowed evaluating the normalized distribution of the beam phase space. The beam has been well described by the Gaussian horizontal profiles (Fig. 6). Its distribution in the vertical scan direction is a combination of the scanning-width-high uniform distribution with symmetric Gaussian edge tails.
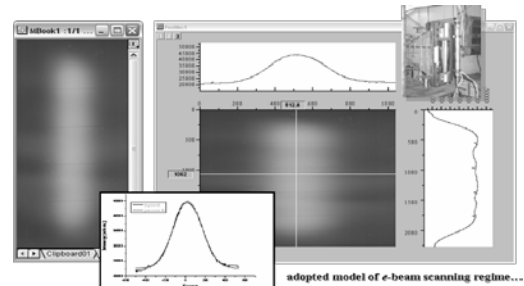

Fig. 6. The digitized scans of the scanning beam monitoring photometry data

For simulations discussed in this section, the lateral Gaussian model obtained from the picture of Fig. 6 has been used in combination with the broad-beam approximation of the scan regime.

Computer simulation of characteristics of a radiation field in the e^--beam irradiated IC was executed by means of the in-house developed Monte-Carlo (MC) code RaT 3.1 [6] taking into account the explicit geometry of IC and the developed model of the scanning source of the linac based irradiation.

2.1. SPATIAL DISTRIBUTIONS OF RADIATION FLUXES

The lateral distribution of the electrons and γ-quanta as measured in a thin planar detector positioned just behind the 4-pipe IC filled with 0.3 g/cm^3 dense SCW are shown in Fig. 7.
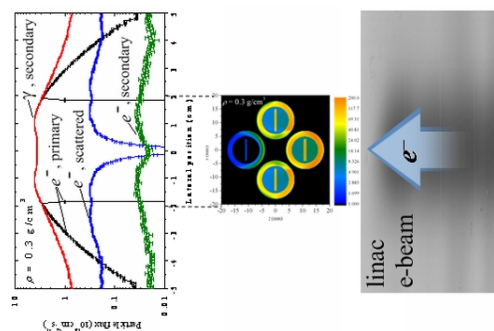

Fig. 7. The lateral distributions of the particle fluxes behind the 7 kW e-beam irradiated IC

The presence of the primary (uncollided) flux of electrons is a direct consequence of application of the realistic model of the scanning beam having definite spatial and angular blurring. It represents the e-beam loss due to its finite spatial and angular spreads.

"Scattered" electrons are those interacted with the IC target and thus strongly scattered laterally.

Secondary electrons are δ-electrons of *e*-beam electrons Möller elastic scattering as well as Compton electrons produced at incoherent scattering of secondary bremsstrahlung photons. Their flux is about one order of magnitude lower then that of scattered electrons. However, they also contribute to the *e*-beam energy deposition, and also can produce isolated radiation defects (Frenkel pairs).

The distinctive feature of Fig. 7 is the very significant gamma flux observed behind the IC. High-*Z* structural materials (from which the IC and samples are made of) transform the IC into an efficient (e^-,γ) converter of ~10 MeV linac *e*-beam. Therefore, samples which are located in the rear pipe of the 4-channel IC, are irradiated mainly with gamma quanta.

2.2. MAPPING OF THE ABSORBED POWER

The Monte Carlo-calculated spatial distributions of the specific power P_{dep} deposited by the linac *e*-beam in the IC are shown in Fig. 8 for two relevant cases of normal and SCW coolant flow. The maps have been built on a rectangular mesh of boxes, 0.2×0.2 mm wide in a horizontal plane (*x*, *z*) and 28 cm (the IC height) long. This resulted in effective axial averaging of P_{dep}.

The maps of Fig. 8,a,b show that major power deposition is located at front parts of three tubes, and in samples these tubes hold. The deposition into water is much smaller as well as the P_{dep} in the back positioned tube. Thus, the deposited power is strongly inhomogeneous and generally spans by two orders of magnitude.

In addition, and with more small-sized spatial resolution, the distribution of P_{dep} was calculated in all samples. One can see from Fig. 8,c that $P_{dep}(x)$ is well symmetric laterally in all samples. It is only weakly dependent on the coolant density due to low-*Z* chemistry of water. The prominent effect is the marginality of P_{dep} in samples located in the rear tube #4. Actually, they can be treated as witness samples at irradiation experiments.
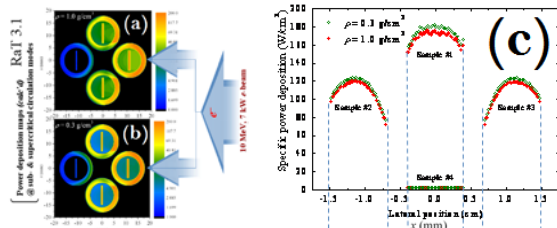
Fig. 8. Axially averaged 2D-maps of the e-beam specific deposited power $P_{dep}(x,z)$ (W/cm^3) in the IC loaded with 0.7 mm thick steel samples and filled with water flow at: normal ($\rho = 1$ g/cm^3) (a); supercritical ($\rho = 0.3$ g/cm^3) (b) conditions; (c) – the correspondent lateral profiles of $P_{dep}(x)$ in samples

Azimuthal distributions of the absorbed power in the IC tubes walls were calculated, at a 1 deg resolution, along a circle $\varphi = 0°...360°$. As shown in Fig. 9, they are also strongly non-uniform. The well-predicted inhomogeneity of the *e*-beam induced heating rate of tubes gives rise to azimuthal gradients of temperature resulting in the correspondent thermal-elastic stress. Thus, the corrosion behavior of the IC tube material under such a diverse irradiation load looks to be also of great interest for radiation material science.
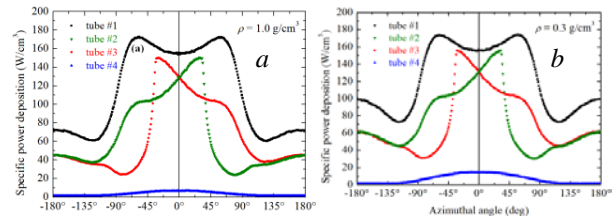
Fig. 9. The azimuth ($\varphi = 0$ along the e-beam axis) dependencies of the specific power deposition $P_{dep}(\varphi)$ for the IC filled with normal water (a) and SCW (b)

2.3. TEMPERATURE FIELDS

The steady state temperature field $T(\mathbf{r})$ inside the disconnected domain Ω of the heterogeneous IC obeys the heat equation (3)

$$\nabla\big(\kappa(\mathbf{r})\cdot\nabla T\big) = P_{dep}(\mathbf{r}), \quad \mathbf{r} \in \Omega, \qquad (3)$$

where $\kappa(\mathbf{r})$ is the thermal conductivity coefficient (we use $\kappa = 17$ W/m-K for steels), $P_{dep}(\mathbf{r})$ is the heat source term, $\mathbf{r}\subset\mathfrak{R}^3(x,y,z)$ for 3D and $\mathbf{r}\subset\mathfrak{R}^2(x,z)$ for 2D calculations of the axially averaged field. The boundary conditions (b.c.) of Eq. 3 at inner (coolant-interfaced) and outer (air-cooled) IC tubes surfaces are the following:

$$\kappa(\mathbf{r})\cdot\frac{\partial T}{\partial \mathbf{n}}\bigg|_{\Gamma_{in}} = \lambda_{in}\cdot(T - T_0), \qquad (4.1)$$

$$\kappa(\mathbf{r})\cdot\frac{\partial T}{\partial \mathbf{n}}\bigg|_{\Gamma_{out}} = \lambda_{out}\cdot(T - T_\infty) + \varepsilon\cdot\sigma\cdot(T^4 - T_\infty^4), \quad (4.2)$$

where $\mathbf{n}$ is the outer normal at the boundaries of component parts, $\lambda_{in,out}$ are the heat transfer coefficients, T_0 and T_∞ are the coolant characteristic temperature and the ambient temperature, respectively. The convective b.c. (4.1) was also used at the boundaries of samples. The radiative term in Eq. 4.2 makes the problem nonlinear.

The coefficients $\lambda_{in,out}$ are model-dependent. For air-cooled IC, $\lambda_{out} = (20...100)$ W·m^{-2}·K^{-1}; the *T*-field is only weakly dependent on λ_{out} at high $T > 350°C$ and the emissivity $\varepsilon \approx 0.5...0.7$ of steels. For conservative estimates, we used $\lambda_{out} = 20$ W·m^{-2}·K^{-1} but also adopted 50 W·m^{-2}·K^{-1} for forced cooling. The coefficient λ_{in} of the heat transfer to a convective flow is taken in the form $\lambda_{in} = Nu\cdot\kappa_0(P,T_0)/D$ [7, 8], where Nu is the Nusselt number, $\kappa_0(P,T_0)$ is the thermal conductivity coefficient of water in a tube of diameter D. In most cases, we assumed the Dittus-Boelter correlation [9].

$$Nu = 0.023\cdot Re^{0.8}\cdot Pr^{0.4}, \qquad (5)$$

where $Re = v\cdot D/v_0(P,T_0)$ and $Pr = v_0(P,T_0)/\kappa_0(P,T_0)$ are the Reynolds and Prandtl numbers, respectively, v is the flow linear velocity, $v_0(P,T_0)$ is its kinematical viscosity.

The speed $v = W/(\rho\cdot S)$ was evaluated from the characteristic data of the natural convection SCWCL System Thermal-Hydraulic (STH) calculations [1, 3]. For thermal calculation of the IC we conservatively adopted $W = 50$ g/s. The characteristic intermediate value of the coolant density $\rho = 0.5$ gm/cm^3 was also assumed.

The Finite Element Method (FEM) 2D and 3D calculations of $T(\mathbf{r})$ followed from the solution of the boundary problem (3), (4) were both performed using the FreeFEM++ 3.13 software [10]. Their essential feature was the consistent application of Monte Carlo cal-

culated $P_{dep}(\mathbf{r})$ mapped onto the 2D/3D meshes of the IC FEM model. Different FEM models of the IC loading have been developed in a strict correspondence with the 3D models of the Monte Carlo simulations. Several options of the 4-pipe IC internal loading have been considered in a series of MC/FEM calculations of temperature fields. In particular, the preliminary models of internal sample holders have been included, and the effects of the IC loading with the samples of different thickness have been studied.

Characteristic results of such calculations for the two-dimensional and three-dimensional IC models are shown in Figs. 10 and 11, respectively. For the 3D case of Fig. 11, the heat source distribution $P_{dep}(\mathbf{r})$ has been calculated by the RaT 3.1 code on a refined mesh with a spatial resolution 0.2×0.2×10 mm.
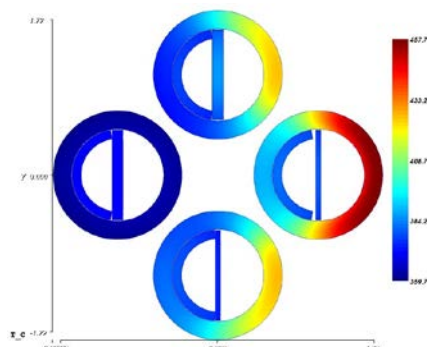

Fig. 10. The temperature field in the 4-pipe IC loaded with a combination of 1 mm and 0.5 mm thick samples. FreeFEM++ 2D calculation

The data shown in Figs. 10 and 11 were obtained for operation mode $P = 23$ MPa, $T_0 = 370°C$, which was assumed for pilot irradiation application of SCWCL model (b). Both 2D and 3D calculations give almost identical (458 and 454°C, respectively) value of maximum temperature T_{max} on the IC frontal surface. Such T_{max} values are acceptable for the IC structural material.
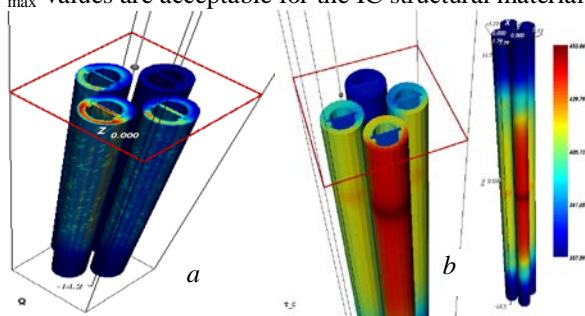

Fig. 11. The Monte Carlo calculated 3D distribution of e-beam deposited power $P_{dep}(\mathbf{r})$ (a) and the temperature field $T(\mathbf{r})$ in the 4-pipe IC (b). FreeFEM++ full 3D calculation

3. EXPERIMENTAL INVESTIGATIONS

The above described four-channel IC was successfully used [2, 3, 5] in the course of four sessions of irradiation of samples of two kinds, Zr–1%Nb and the weld joined Ni–Cr Inconel 690/In52MSS, by ~10 MeV electrons (total sessions duration 574 h, incl. 497 h under *e*-beam, the IC surface fluence was up to $10^{20}\ e^-/cm^2$). The all-welded SCWCL model (b) operation mode was the following: pressure $p = 23.5$ MPa, coolant temperature $T < 380°C$, coolant mass-flow rate $W > 50$ g/s.

Quantitative data which characterize the irradiation conditions are presented below in this section.
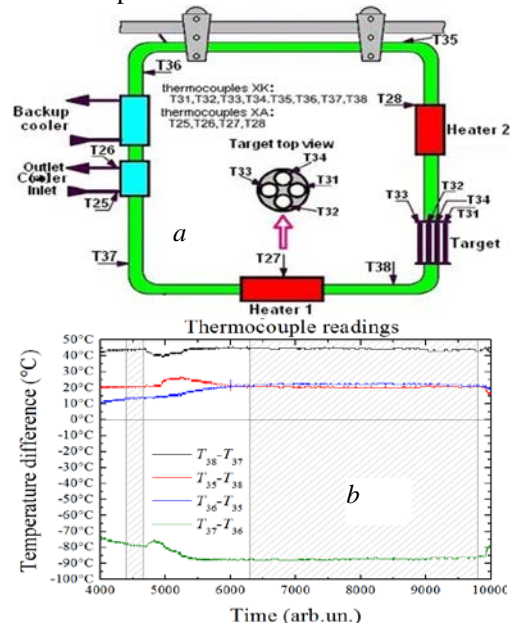

Fig. 12. The schematics of the experimental measurements of temperatures (a) and typical and measured data for the temperature differences along the loop contour at natural circulation (b)

Temperature measurements were carried out using a set of Chromel-Copel (CCT, XK) and Chromel-Alumel (CAT, XA) thermocouples fastened on the external surface of piping near the corners of SCWCL, at heaters, coolers, and also close to the top of the IC behind the irradiated zone (Fig. 12,a). The thermocouple readings were digitally recorded, as shown in Fig. 12,b.

These primary results definitely show that the circulation occurs counterclockwise. However, the magnitude of temperature drops reaches dozens degrees centigrade. This *ex facte* violates the predictions [1, 3] of the SCWCL STH model since the as-measured data point to the very much lower mass-flow rate W of the coolant.

From the STH theory point of view, we ventured to treat these discrepancies as non-controlled drifts, under irradiation, of the readings of thermocouples calibrated at normal conditions. Physical reasons of such drifts are not yet clear. They can follow from the defects of fastening, non-harmonized thermal expansion, chemical transformations under irradiation in an aggressive ozone and nitric acid environment, and so on.
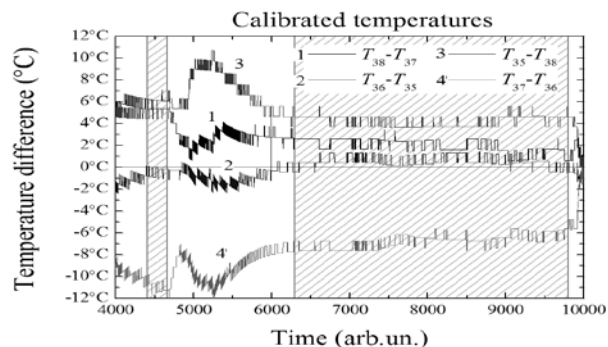

Fig. 13. The recalibrated data on the temperature drops

In order to eliminate the assumed drifts, the in-place recalibration procedure was applied. The SCWCL circulation flow has been carefully relaxed along the well-

known Widom line $T_{saturation}(p)$ of the water coolant phase diagram. The obtained primary readings of thermocouples have been used to calculate the calibration curves which were found to be practically linear. When applying these calibration functions to the routine measurements, the temperature differences contracted (see Fig. 13 *cf.* Fig. 12,b) to the 5...10°C wide range well compatible with the STH model calculated $W \approx 80$ g/s.

3.1. IRRADIATION RECORDS ANALYSIS

Naturally, actual conditions of the irradiation experiment differed from the nominal ones (10 MeV/7 kW) assumed in section 2 at characterization of the multichannel IC design. Therefore, actual irradiation records (shown in Figs. 14 to 17) were applied to the analysis of experimental results [3, 5].

As recorded in Fig. 14, the irradiation lasted for 497 h and 20 min but was not totally continuous. The uninterruptible 24/7 regime of the beam load has been reached at the 3rd week only and lasted for 2 weeks.

The *e*-beam current (see Fig. 15,a) and power (see Fig. 16,a) experienced the trend of systematic decrease. It is explained by the operators policy to prevent the loop overheating basing on the uncalibrated readings of the IC-located thermocouples. According to the records of Fig. 15,b, the total number of the linac-emitted electrons amounts to 6.4×10^{21} for this experiment.
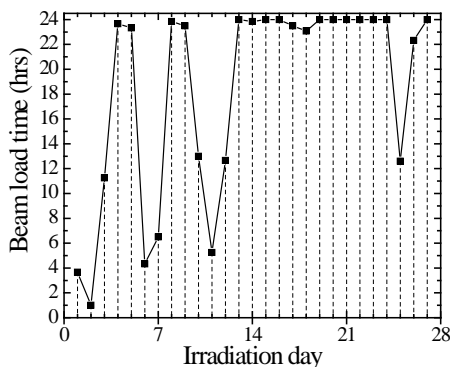

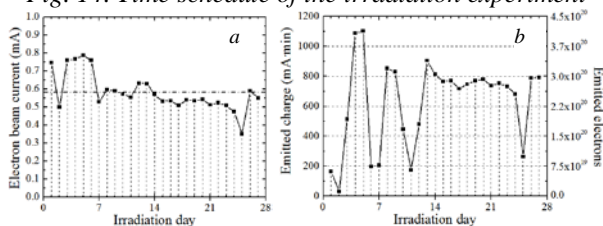Fig. 14. Time schedule of the irradiation experiment

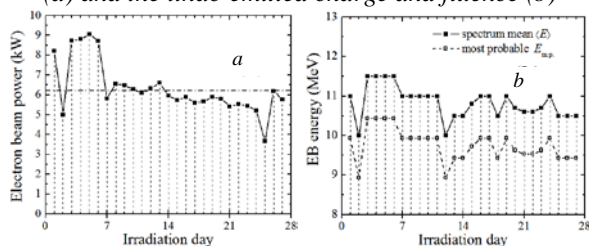Fig. 15.TPer-day records of the LPE-10 mean current (a) and the linac-emitted charge and fluence (b)

Fig. 16. Per-day records of the LPE-10 mean electrical power (a), the measured mean energy ⟨E⟩ (bold markers), and the most probable energy $E_{m.p.}$ (open markers) estimated for the e-beam reference spectrum [11] (b)
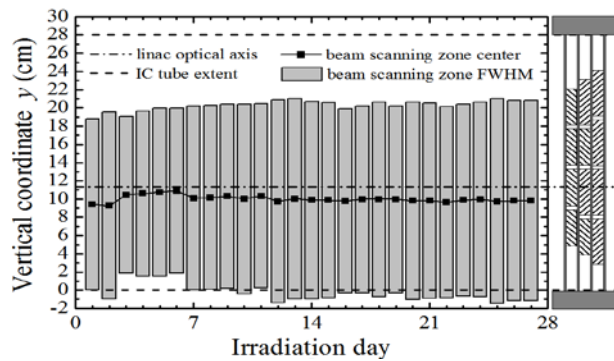

Fig. 17. Per-day monitored parameters of the spatial distribution of the scanning e-beam in confrontation to the locations of specimens in the 4-pipe irradiation cell

The *e*-beam energy spectrum mean energy ⟨E⟩ (see Fig. 16,b) was monitored on-line using the technique described in ref. [12]. The characteristics of the spatial distribution of the *e*-beam scanning regime were also recorded on-line and visualized by means of the SCWCL automated control system [13]. Fig. 17 shows that they are also time dependent and manifest the systematic shift of the beam scanning zone center down from the IC horizontal midplane. Such an offset strongly affects the absorbed dose spatial distributions. Therefore, it has been properly considered in the computer model developed for processing of the results of this experiment.

3.2. THE SCANNING BEAM PHASE SPACE

The LPE-10 linac scanning beam is an extended source of primary electrons with complex spatial and angular distribution. To characterize the specific irradiation session, it is crucial to model it as accurately as possible. Thus, dedicated photometric measurements had been conducted, and an appropriate fit of the measured data has been developed for the RaT 3.1 MC code.

The linac exposed glass plates positioned before and behind IC (Fig. 18,a) have been scanned and digitized (see Fig. 18,b). The obtained arrays of 2D primary flux distributions have been fitted with a Gaussian based nonlinear least-square (LSQ) fit model, as compared, in Fig. 18,c and Fig. 19, to measurements data.
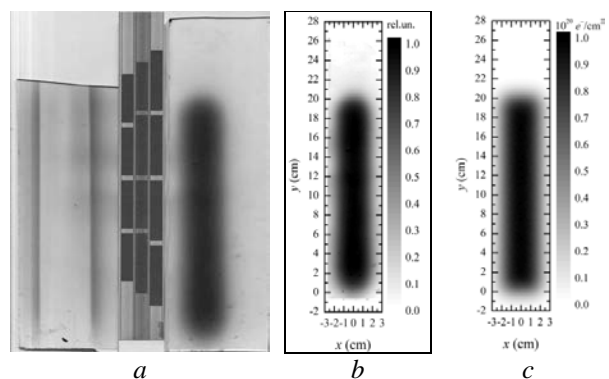

Fig. 18. The scans of the back and front glass plates exposed by the LPE-10 e-beam and combined with the scheme of the samples loading in the IC (a) and the images of the spatial distribution on the front plane: as digitized (b) and as reconstructed by the RaT 3.1 code primary particle generator (c)
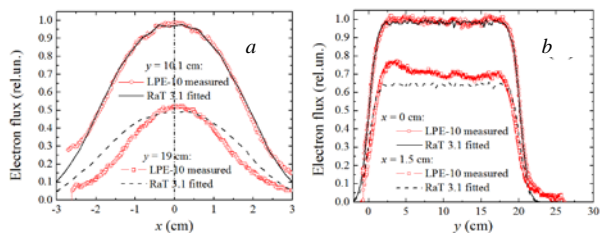
Fig. 19. The results of the reconstruction of the lateral (vs. Ox, a) and axial (vs. Oy, b) spatial distributions of the LPE-10 scanning beam by the RaT code fitting model. The data for y = 10.1 cm and x = 0 cm correspond to the central part of the scanning zone. The complementary data at y = 19 cm and x = 1.5 cm describe the fits for top and right edges of the distributions shown in Figs. 18,b,c

3.3. THE IC ABSORBED POWER

The Monte Carlo-simulated fine resolved spatial distribution of the deposited power P_{dep} (W/ cm^3) inside the 4-pipe IC are illustrated in Fig. 20. Top view data, depth profiles across the front and back positioned tubes, and lateral distributions in the specimens contained planes are shown using the same color mapping scale. The specific power deposition amounts to 150 W/cm^3 at 6.23 kW$_e$ mean power of linac e-beam irradiation.

The P_{dep} mapping data of Fig. 20 look similar to those of sec. 2.2 but reveal a lot of details implied by the specific loading of tubes with different specimens.

Besides, these data open the possibility of consistent calculation of the temperature field in which the irradiated samples interacted with the corrosive coolant.
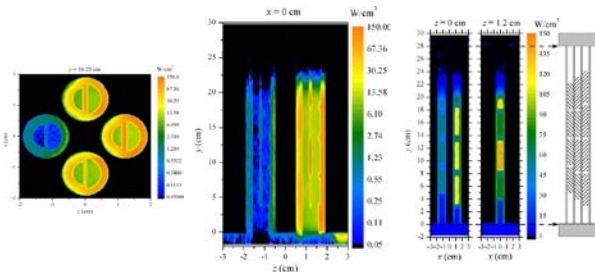

Fig. 20. 3D spatial distribution of the selected cross-sections of the power deposition in the 4-pipe IC

3.4. THE IC TEMPERATURE FIELD

For multi-channel IC, temperature profiles in different tubes differ due to the non-uniform power absorption, both directly in a water flow and, mainly, in irradiated tubes and samples. The MC/FEM calculated 3D temperature field of the IC is shown in Fig. 21.
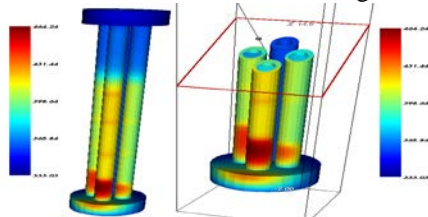

Fig. 21. The MC/FEM-calculated temperature field in the 4-channel irradiation cell

The peak temperature amounts to $T_{max} = 464$°C (450…460°C of the sec. 2.3 calculations with nominal irradiation parameters). The maximal value is reached in

a somewhat unexpected location, the bottom part of the front tube near the flange. This is due to the enhanced (to 3 mm) thickness of this part of the IC when the sample holding cassette was inserted. Much smaller local overheats of the same nature are traced at the gaps between the vertically spaced samples.

Due to the IC air cooling, the calculated temperatures of the top (just below the upper flange) parts of the IC tubes are close to the convection loop inlet temperature $T_{in} = 360$°C despite of the coolant heating.

This is just the place where the monitoring thermocouples (see T31-T34 in Fig. 12,a) were located at irradiation. Their recorded readings ranged from 345 to 375°C, and the reference temperature (360°C) has been chosen in the midst of this range. The observed ±15°C scattering is possibly due to variations of the e-beam power (see Fig. 16,a), water flow instabilities, and the irradiation impact on the state and behavior of thermocouples.

It is worth noting that the data of Fig. 21 represent the time-averaged (over the whole irradiation experiment timeline shown in Figs. 14-17) thermal field of the multi-channel IC having $T_{max} = 464$°C. Such a field is descriptive from the point of view of interpretation of corrosion behavior of irradiated samples. However, it ignores inevitable (and, in particular, accidental) fluctuations of temperature.

Certain indirect data follow from the appearance of the IC after the completion of irradiation experiment (Fig. 22) and point to its local overheating to much higher temperatures if we judge by the coloring of the frontal central tube. During the irradiation week 1, there was a case of equipment failure when the linac was switched off and the water circulation was automatically stopped. The subsequent beam-on procedure assumes check-ins of coolant fill-up and its preliminary heating by the SCWCL heater. Though these conditions had been accidentally violated one day at the initial stage of the pilot irradiation, the short-time tube overheating to $T > 500$°C (roughly estimated from the heat scale visible on the tube surface) did not resulted in the breakdown of the pressurized irradiation zone. This confirms sufficient safety margins of the irradiation cell design.

Fig. 22. Appearance of the IC after the termination of irradiation sessions

CONCLUSIONS

We present a simple but sophisticated design of the multi-channel irradiation cell for *in situ* irradiation of macroscopic samples of materials by ~10 MeV relativistic electrons inside the convective water flow of high pressure and temperature. The design is highly optimized and well characterized by means of computer Monte Carlo and Finite Element Method modeling.

The safety and durability of the proposed irradiation cell has allowed us to carry out the world first irradiation of Ni–Cr and Zr based alloys in the close vicinity of the water coolant critical point. The results obtained are of great value for GenIV Supercritical Water-Cooled Reactor structural materials feasibility assessment.

We consider valuable experience obtained at operation of the irradiation cell and circulation loop under irradiation as a basis of future irradiation experiments planned at NSC KIPT Electron Irradiation Test Facility.

REFERENCES

1. A.S. Bakai, V.N. Boriskin, A.N. Dovbnya, et al. Supercritical water convection loop (NSC KIPT) for materials assessment for the next generation reactors // *Proc. of the 5th Int. Symposium on Supercritical Water-Cooled Reactors (ISSCWR-5).* Vancouver, BC, Canada, Mar. 13-16, 2011. On CD-ROM, Paper № 51.
2. A.S. Bakai, V.N. Boriskin, M.I. Bratchenko, et al. Electron irradiation of the material samples of new generation nuclear reactors in the supercritical water convection loop // *Problems of Atomic Sci. and Tech. Series "Nuclear Physics Investigations".* 2013, № 6, p. 230-234.
3. A.S. Bakai, V.N. Boriskin, A.N. Dovbnya, et al. Supercritical Water Convection Loop for SCWR materials corrosion tests under electron Irradiation: First results and Lessons learned // *Proc. of the 6th Int. Symposium on Supercritical Water-Cooled Reactors (ISSCWR-6),* Shenzhen, Guangdong, China, Mar. 3-7, 2013. On CD-ROM, Paper № 13062.
4. *The rules for calculating the strength of stationary boilers and steam and hot water.* RD 10-249-98. Moscow. 1999.
5. A.S. Bakai, V.N. Boriskin, A.N. Dovbnya, et al. Combined effect of irradiation, temperature, and water coolant flow on corrosion of Zr-, Ni-Cr-, and Fe-Cr-based alloys // *Proc. of the 7th Int. Symposium on Supercritical Water-Cooled Reactors (ISSCWR-7),* March 15-18, 2015, Helsinki, Finland. Paper № ISSCWR7-2012, p. 14.
6. M.I. Bratchenko, S.V. Dyuldya, M.A. Skorobogatov. RaT, a multi-purpose code for Monte Carlo modeling of dosimetric quantities // *Abstr of the 4th Conf. on High-Energy Physics, Nuclear Physics and Accelerators.* February 27-March 3, 2006, Kharkov, Ukraine, p. 80.
7. Natural circulation data and methods for advanced water cooled nuclear power plant designs // *IAEA-TECDOC-1281. IAEA.* Vienna, 2002, p. 252.
8. I.L. Pioro, H.F. Khartabil, R.B. Duffey. Heat transfer to supercritical fluids flowing in channels – empirical correlations (survey) // *Nuclear Engineering and Design*, 2004, v. 230, p. 69-91.
9. F.W. Dittus, L.M.K. Boelter. Heat transfer in automobile radiators of the tubular type // *University of California Publications in English*, Berkeley. 1930, v. 2, p. 443-461.
10. D. Bernardi, F. Hecht, K. Ohtsuka, O. Pironneau. *FreeFEM++ Manual.* http://www.freefem.org/ff++.
11. A.N. Dovbnya, A.I. Zykov, Eh.S. Zlunitsyn, et al. Radiation field creation at the electron linac LPE-10 for long-term tests of structural materials under Molten-Salt Reactor conditions // *Problems of Atomic Sci. and Tech. Ser. "Nuclear Physics Investigations".* 2006, № 2, p. 187-189.
12. V.N. Boriskin, A.N. Dovbnya, L.K. Myakushko, et al. Operational control of an average beam energy at a technological electron linac // *Problems of Atomic Sci. and Tech. Series "Nuclear Physics Investigations".* 2006, № 2, p. 117-119.
13. V.N. Boriskin, V.A. Momot, S.K. Romanovsky, et al. Supercritical water convection loop control system // *Problems of Atomic Sci. and Tech. Series "Nuclear Physics Investigations".* 2014, № 3, p. 82-85.

Article received 30.04.2015

МНОГОКАНАЛЬНАЯ КАМЕРА ДЛЯ ОБЛУЧЕНИЯ ЭЛЕКТРОНАМИ ОБРАЗЦОВ МАТЕРИАЛОВ В СВЕРХКРИТИЧЕСКОЙ ВОДНОЙ КОНВЕКЦИОННОЙ ПЕТЛЕ

А.С. Бакай, В.Н. Борискин, М.И. Братченко, Ю.В. Горенко, А.Н. Довбня, С.В. Дюльдя, Г.Г. Ковалев

В ХФТИ создана суперкритическая водяная конвекционная петля с четырехканальной камерой облучения. Петля размером 1,2×1,5 м изготовлена из нержавеющей стали. Установка позволяет проводить коррозионные тесты кандидатных конструкционных материалов реакторов IV поколения с сверхкритическим водным охлаждением под облучением. Образцы в потоке воды при 350…400°C, 23…25 МПа облучаются электронным пучком 10 МэВ/10 кВт линейного ускорителя ЛУЭ-10. Приводятся результаты использования четырехканальной камеры во время 500-часового сеанса облучения образцов циркония и инконеля.

БАГАТОКАНАЛЬНА КАМЕРА ДЛЯ ОПРОМІНЕННЯ ЕЛЕКТРОНАМИ ЗРАЗКІВ МАТЕРІАЛІВ У НАДКРИТИЧНІЙ ВОДЯНІЙ КОНВЕКЦІЙНІЙ ПЕТЛІ

О.С. Бакай, В.М. Боріскін, М.І. Братченко, Ю.В. Горенко, А.М. Довбня, С.В. Дюльдя, Г.Г. Ковалев

У ХФТІ створена суперкритична водяна конвекційна петля з чотирьохканальною камерою опромінення. Петля розміром 1,2×1,5 м виготовлена з нержавіючої сталі. Установка дозволяє проводити корозійні тести кандидатних конструкційних матеріалів реакторів IV покоління з надкритичним водяним охолодженням під опроміненням. Зразки в потоці води при 350…400 °C, 23…25 МПа опромінюються електронним пучком 10 МеВ/10 кВт лінійного прискорювача ЛПЕ-10. Наведено результати використання чотирьохканальної камери під час 500-годинного сеансу опромінення зразків цирконію та інконелю.